Geophysical Research Letters

Supporting Information for

Big Jump of Record Warm Global Mean Surface Temperature in 2014-2016 Related to Unusually Large Oceanic Heat Releases

Jianjun Yin[1,2,3], Jonathan Overpeck[4], Cheryl Peyser[1] and Ronald Stouffer[1]

1. Department of Geosciences, University of Arizona

2. Program in Atmospheric and Oceanic Sciences, Princeton University

3. GFDL/NOAA

4. School for Environment and Sustainability, University of Michigan

Contents of this file

Introduction

The supporting information consists of thirteen supplementary figures and two supplementary tables that are referred to in the main text.

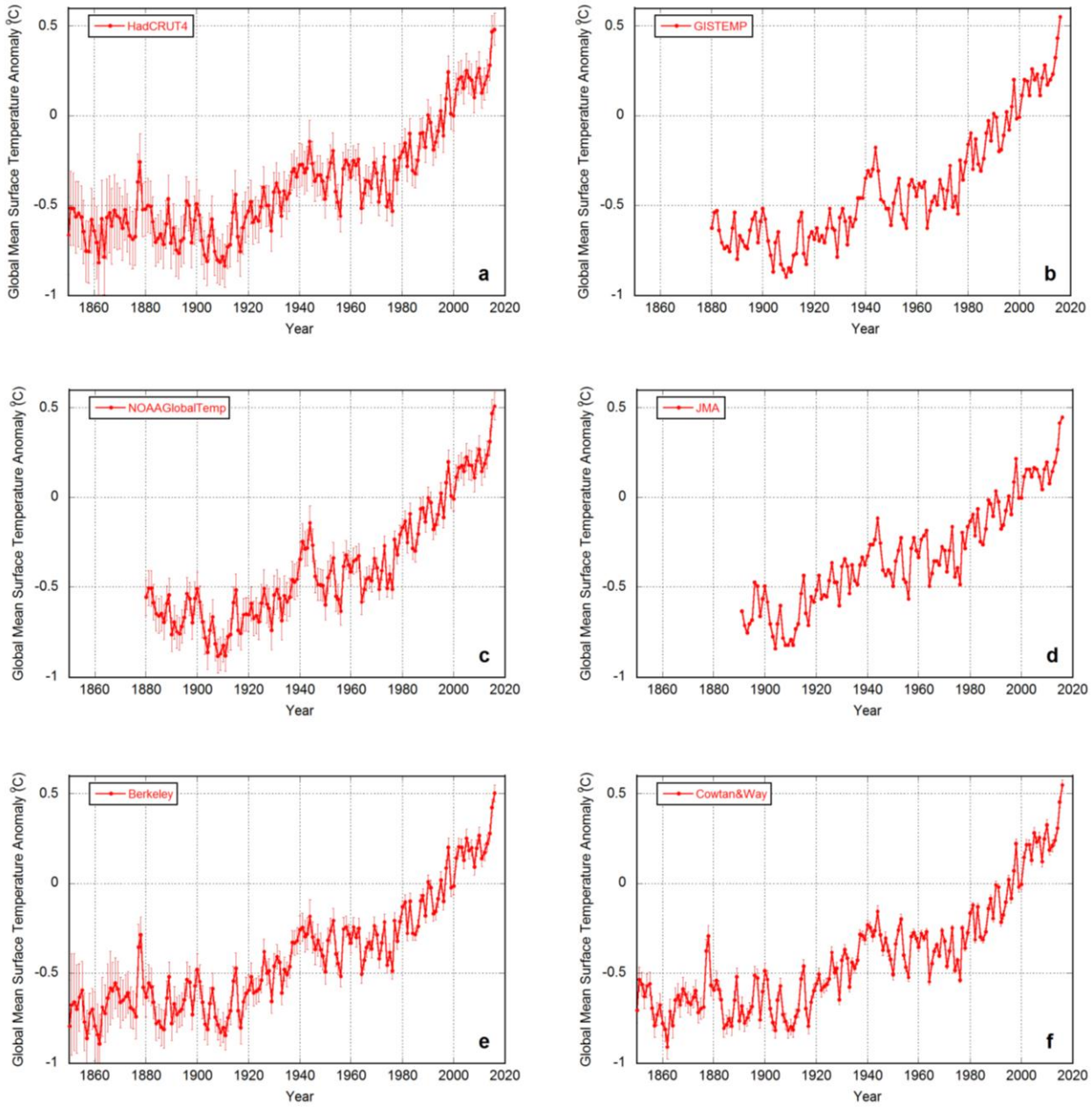

Figure S1. Six available GMST datasets and their uncertainty estimates. (a) HadCRUT4. Uncertainties are computed by integrating across the distribution described by 100 ensemble members. Additional uncertainties resulting from measurement and sampling error and coverage uncertainty are also included. (b) GISTEMP. (c) NOAAGlobalTemp. Uncertainties are estimated as the standard error. (d) JMA. (e) Berkeley. Uncertainties indicate the 95% confidence interval for statistical and spatial undersampling effects as well as ocean biases. (d) Cowtan&Way. The error bars show total uncertainty (1σ). See the references for more details.

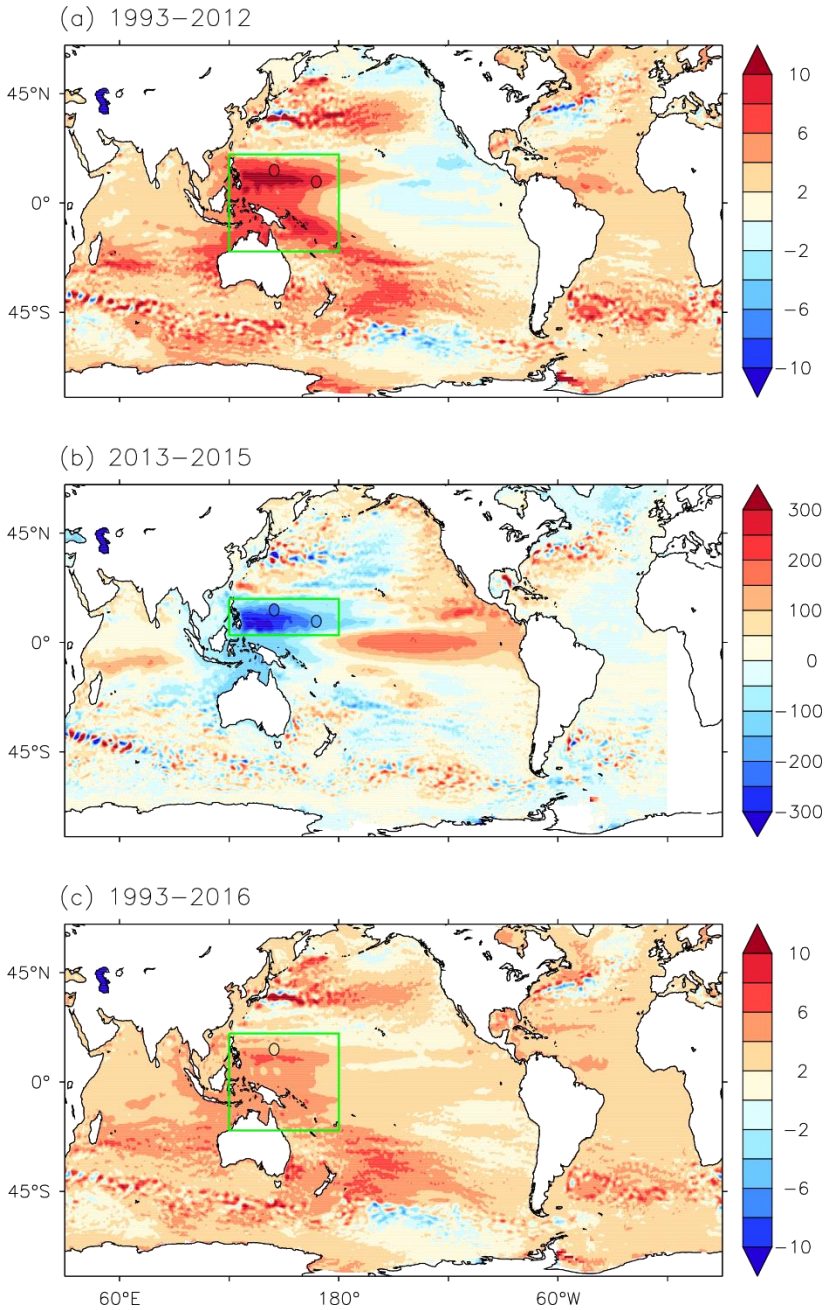

Figure S2. Sea level changes during 1993-2016 from the altimetry data (AVISO). (a) Linear trend (mm yr^{-1}) of sea level during 1993-2012. (b) Sea level change (mm) during 2013-2015. (c) Linear trend (mm yr^{-1}) of sea level during 1993-2016. The colored circles indicate the values from the two tide gauge data at Kwajalein and Guam. The green boxes in (a) and (b) indicate WP and NWP, respectively. Note that the 2013-2015 heat release from WP and the related sea level drop significantly altered the long-term sea level rise pattern in the tropical Pacific. By comparing (a) and (c), the once fastest sea level rise center in the WP especially east of the Philippines largely disappeared after the 2013-2015 event.

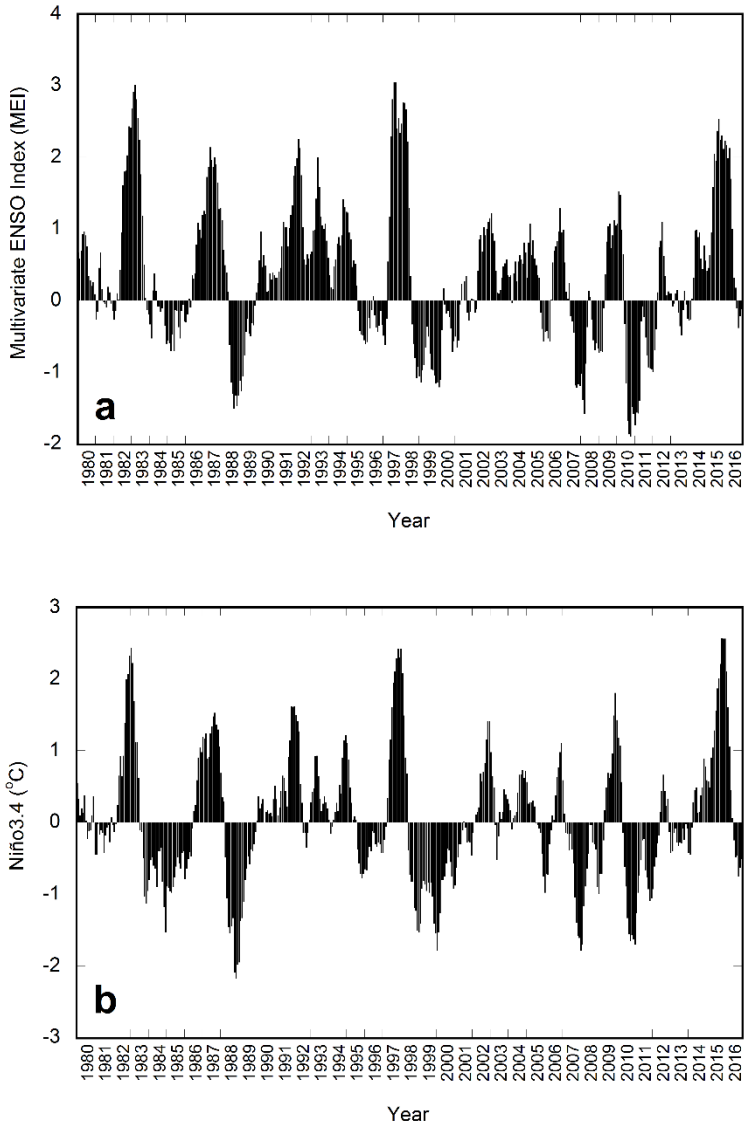

Figure S3. Time series of ENSO indices - MEI (a) and Niño3.4 (b). Monthly values from January 1980 to December 2016 are used for both indices.

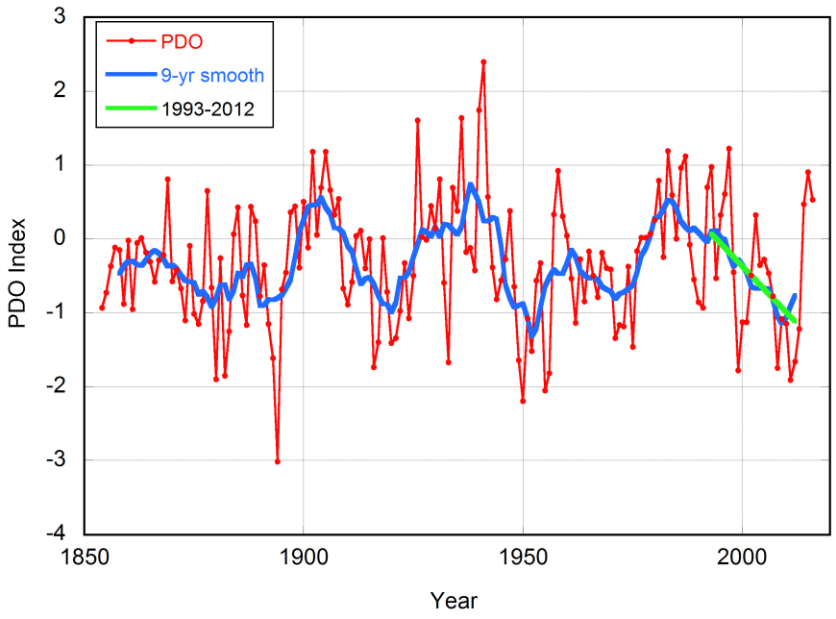

Figure S4. Time series of the observed PDO index during 1854-2016. The data are from NOAA NCEI. Both the annual mean (red) and 9-year low-pass filtered (blue) values are shown. The green line is the linear trend of the filtered PDO index during 1993-2012. The IPO index (not shown) resembles the PDO index. The regression analyses based on the PDO or IPO indices generate similar results.

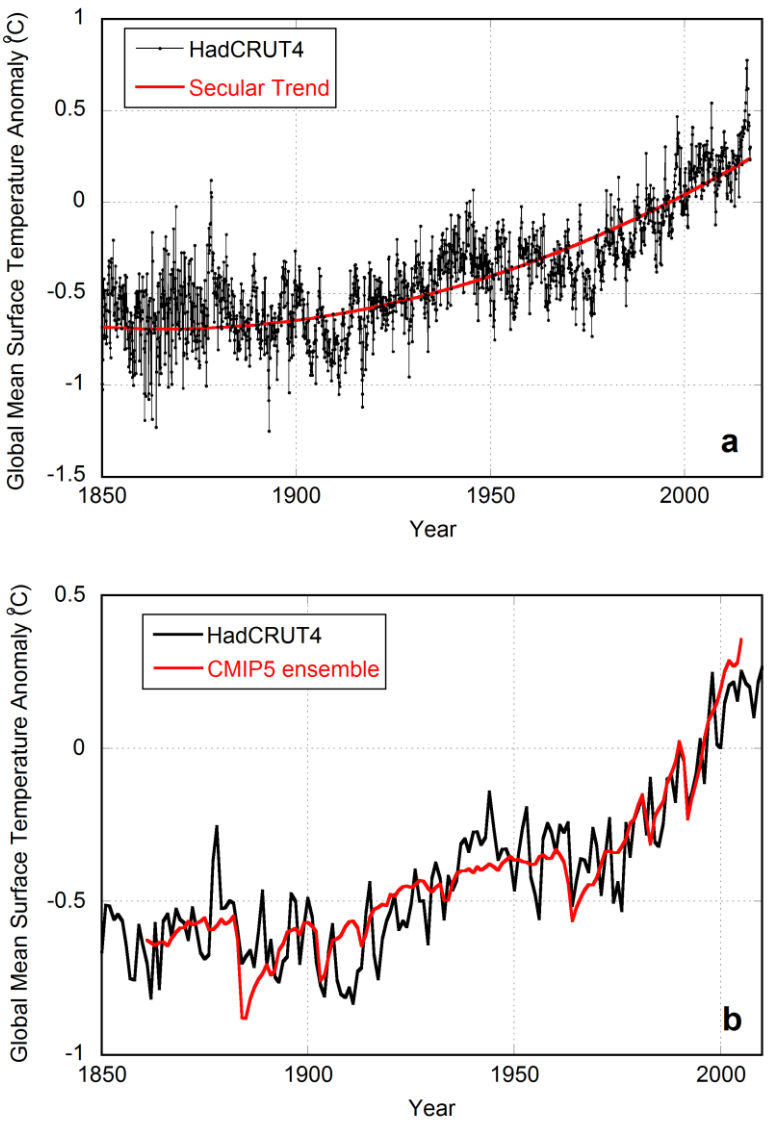

Figure S5. Estimates of internal variability of GMST with two methods. (a) Separation of the nonlinear secular trend from the monthly HadCRUT4 dataset using the Ensemble Empirical Mode Decomposition. The detrended annual mean HadCRUT4 time series show a standard deviation of about 0.12°C. Similar analysis can be applied to other GMST datasets. (b) The ensemble mean of annual GMST anomalies in the historical runs of 40 CMIP5 models after calibration with the HadCRUT4 data. This estimate of the forced response of GMST is removed from the annual HadCRUT4. The time series of the residual show a standard deviation of 0.11°C. Therefore, internal GMST variability estimates are consistent based on the two methods.

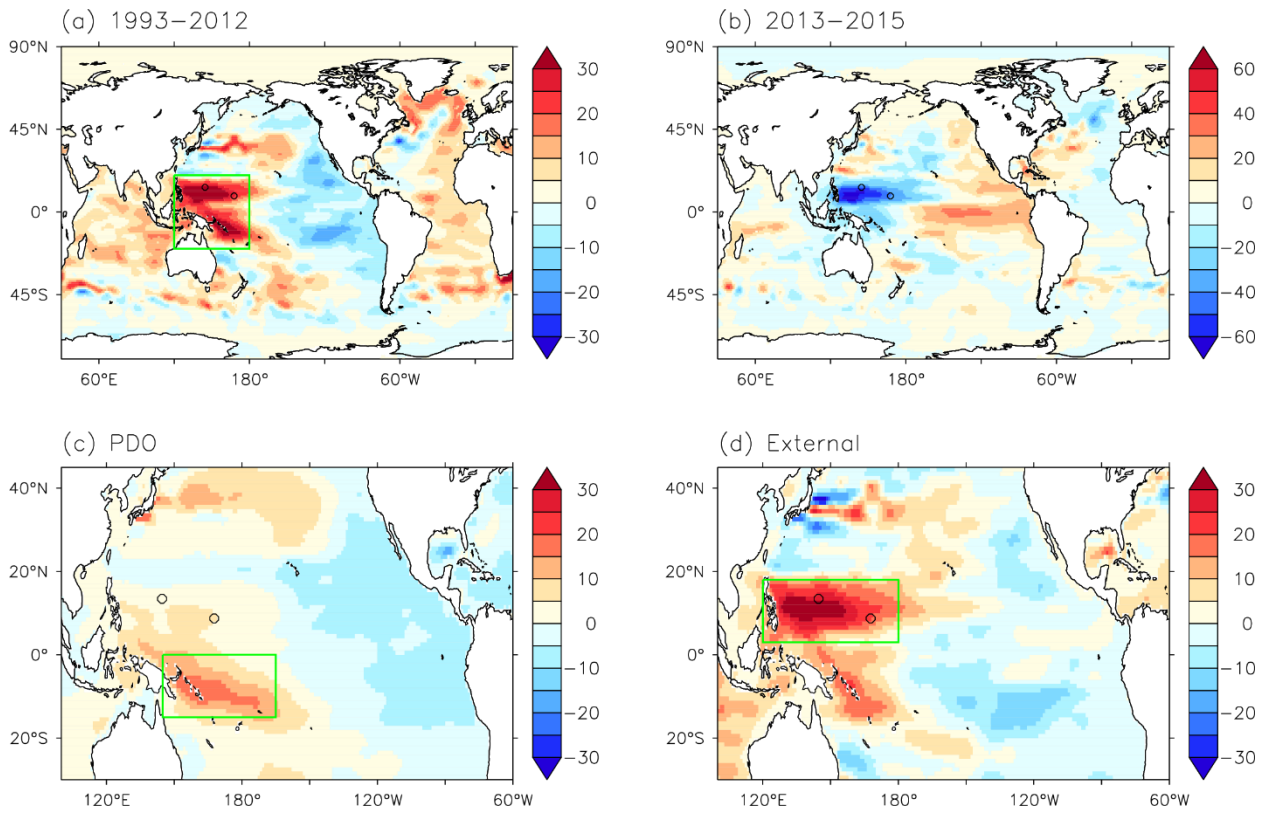

Figure S6. Same as Figure 2, but with the Ishii OHC data for the upper 700 m.

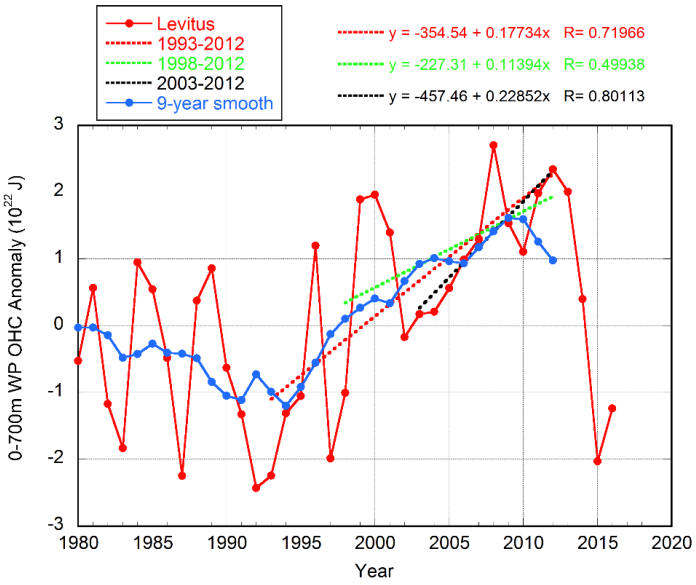

Figure S7. Ocean heat accumulation and release in the upper 700 m of the WP. The linear trends of OHC are compared for different periods before 2013. The 9-year running mean (blue curve) indicates that the gradual heat buildup in the WP started from 1993-1994.

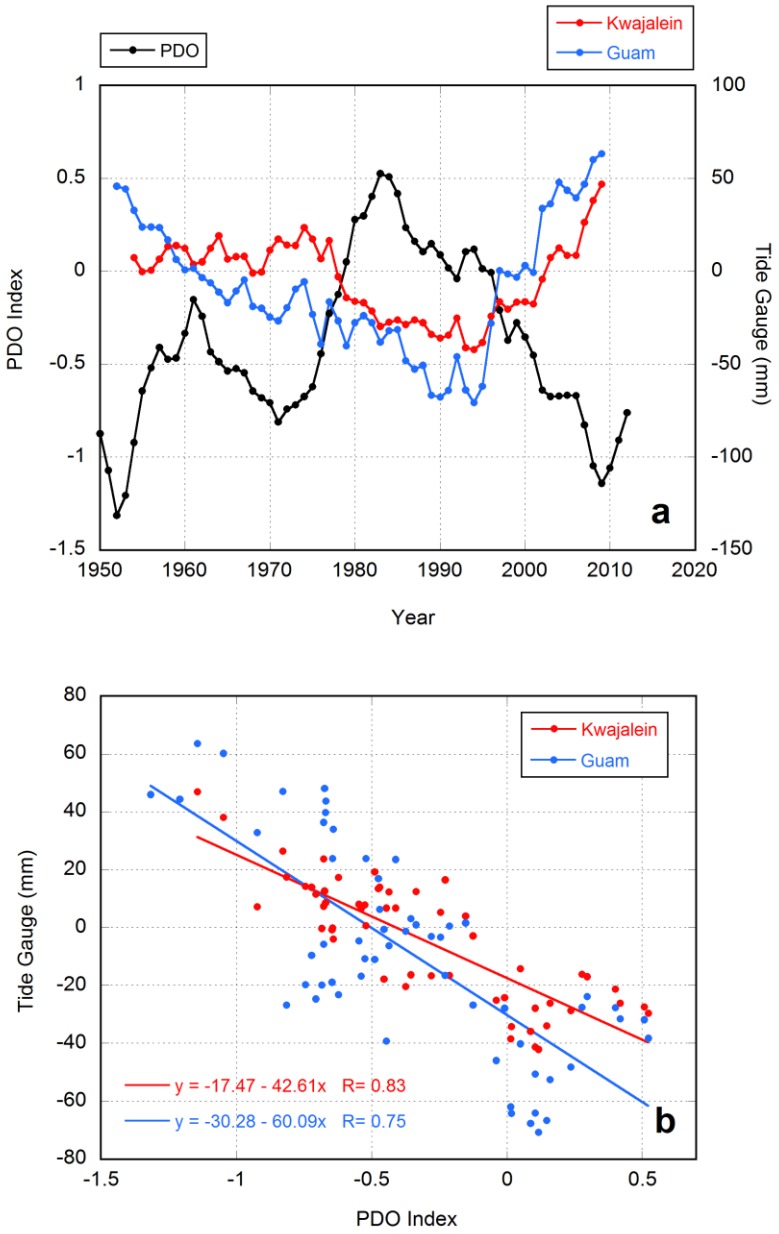

Figure S8. Relationship between the observed PDO index and tide gauge data in the NWP. (a) Time series of the low-pass filtered PDO index and two tide gauge data at Kwajalein and Guam. The global mean sea level is first removed from the tide gauge data. Then the residual time series are detrended linearly before a 9-year low-pass filter is applied. (b) Correlation and regression between the PDO index and the detrended tide gauge data.

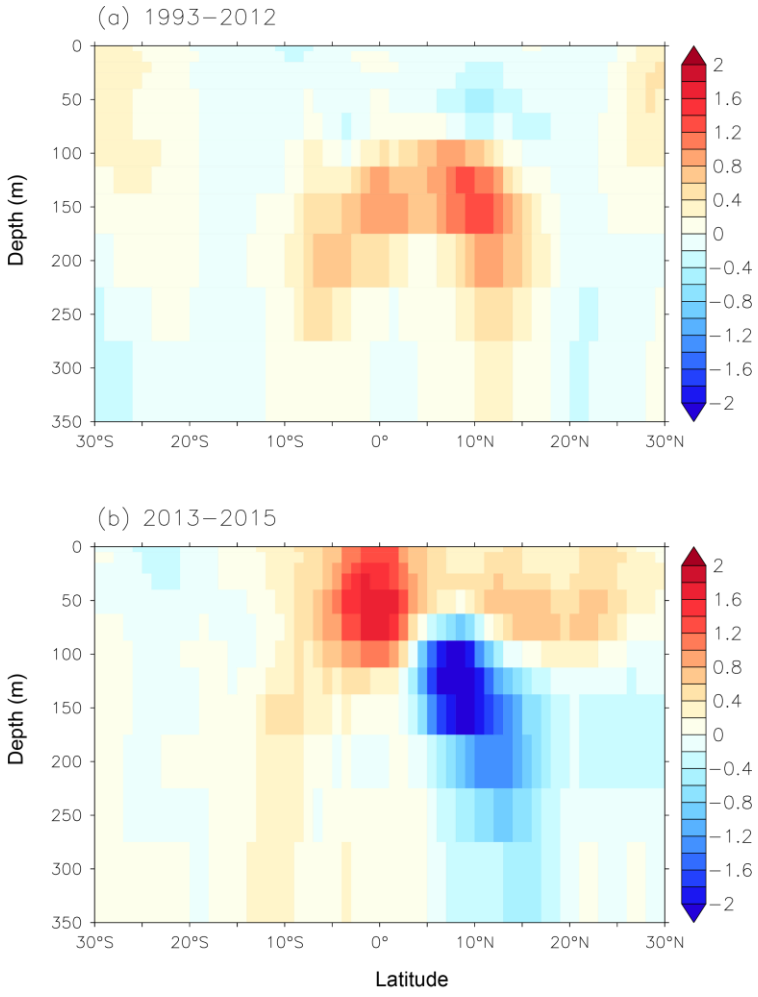

Figure 9. Zonal mean ocean temperature changes (°C) across the Pacific Ocean as a function of depth and latitude (Levitus data). (a) Interdecadal ocean temperature changes during 1993-2012 based on the linear trend. (b) Interannual ocean temperature changes during 2013-2015.

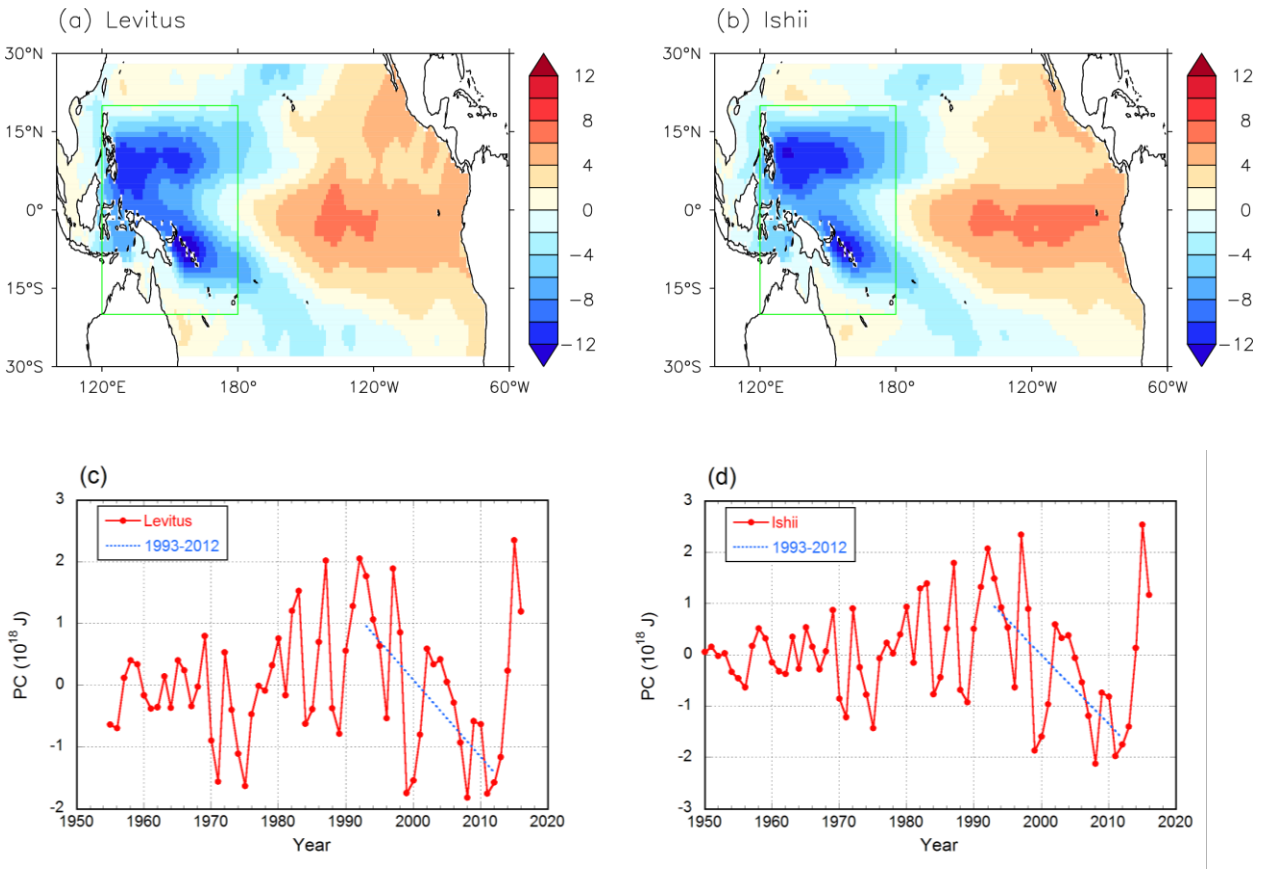

Figure S10. EOF1 (a, b) and PC1 (c, d) of the observed OHC in the tropical Pacific. Both the Levitus and Ishii datasets are shown. The green boxes in (a) and (b) indicate WP. Blue dashed lines in PC1 show its linear trend during 1993-2012. EOF1 explains 37% and 42% of the total variance in the Levitus and Ishii data, respectively.

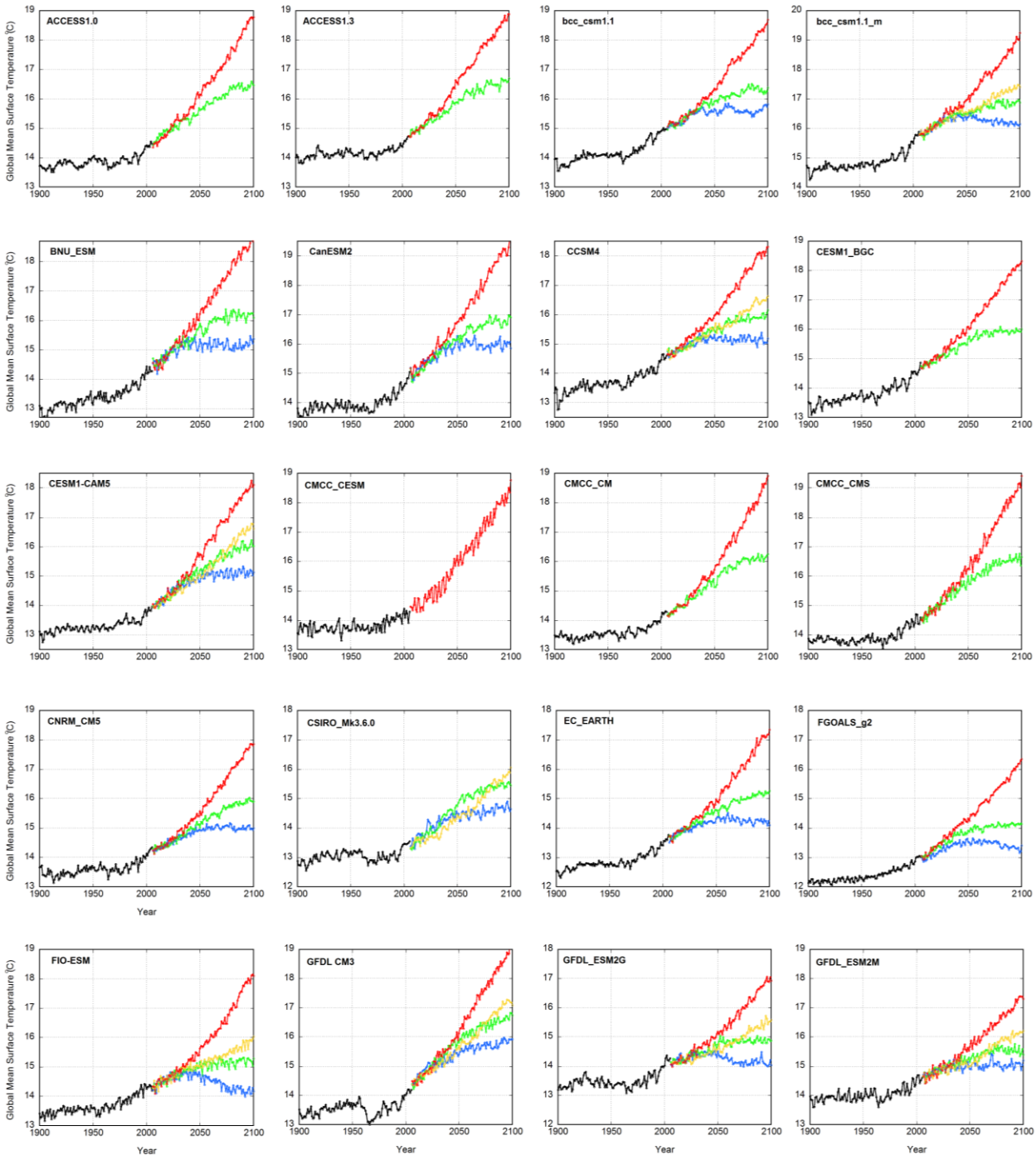

Figure S11. GMST time series in the historical simulations and RCP projections of 40 CMIP5 models. Black-historical, blue-RCP2.6, green-RCP4.5, yellow-RCP6.0 and red-RCP8.5. The models and available data are summarized in Table S1.

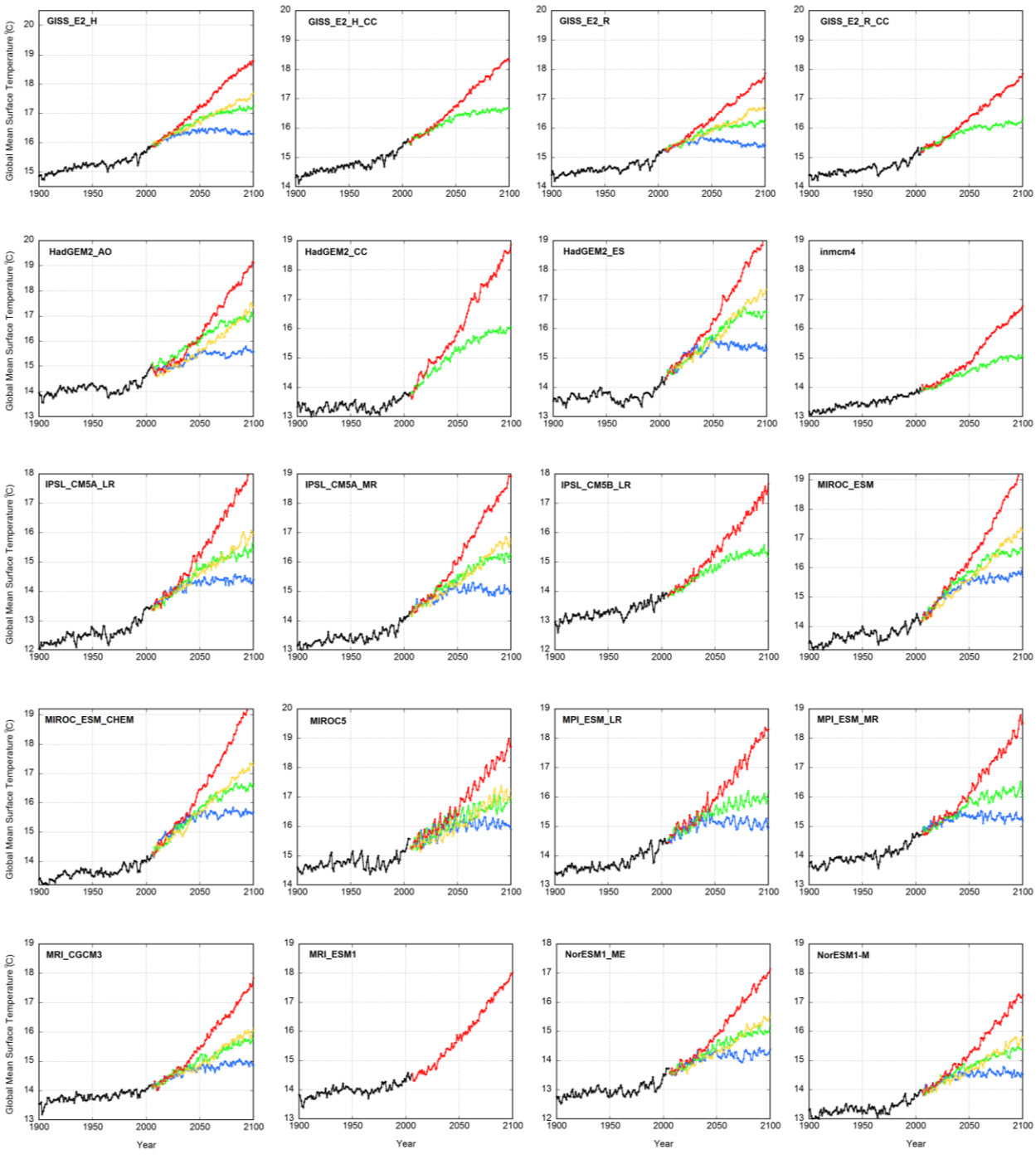

Figure S11. (continued)

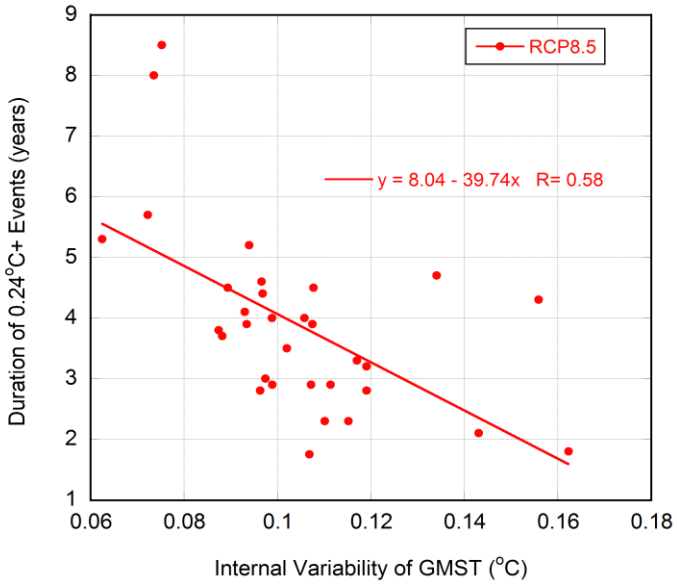

Figure S12. Relationship between the duration of the 0.24°C+ event and internal variability of GMST. The scenario considered here is RCP8.5. Internal variability of GMST is evaluated using 200-year piControl simulations of the CMIP5 models. Each dot indicates one CMIP5 model result. The line is the linear fit. See Table S2 for more information.

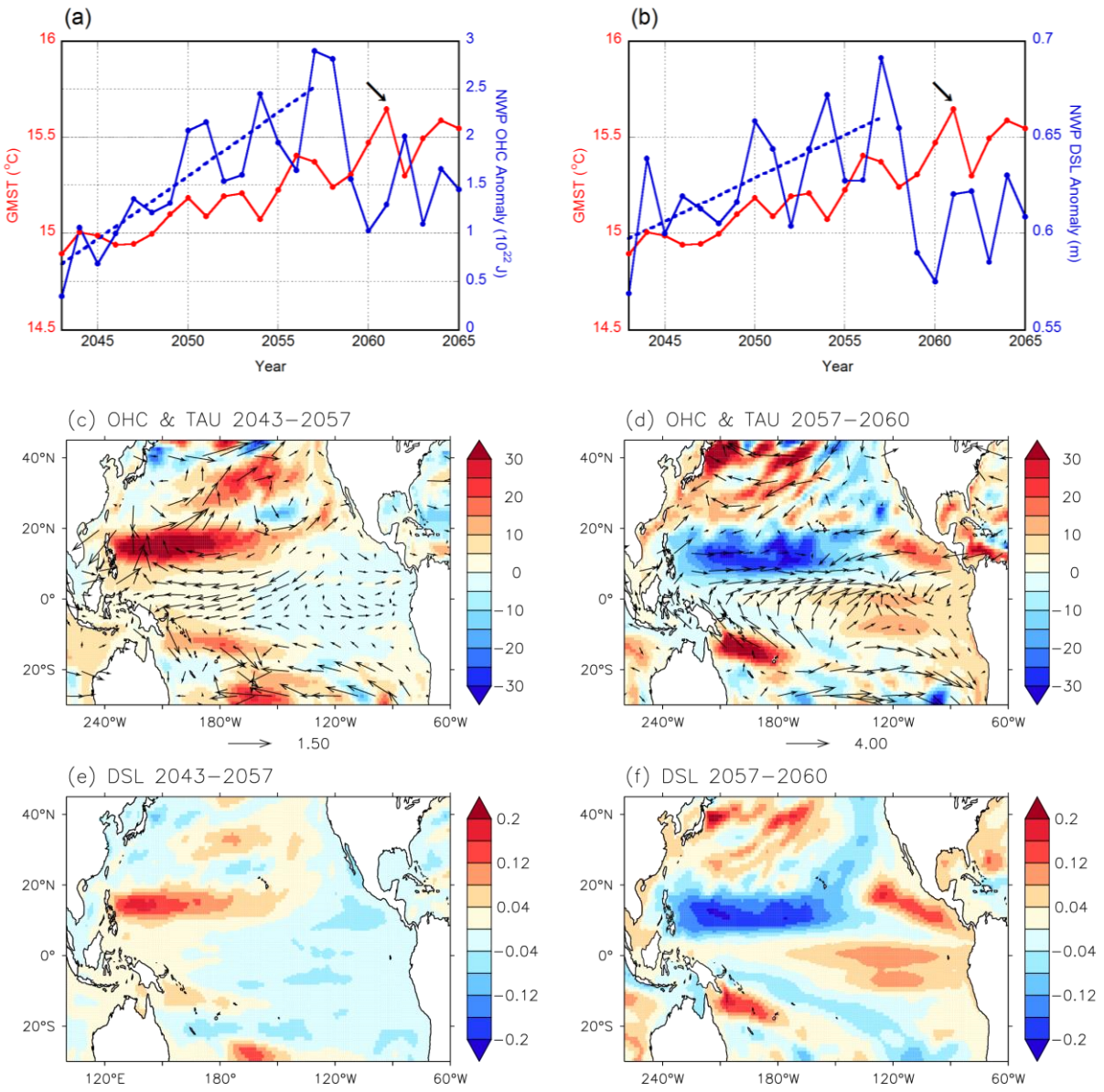

Figure S13. A 0.24°C+ event in the GFDL ESM2G projections under RCP8.5. The event occurs in 2060-2061 with a record-breaking magnitude of 0.24°C. OHC analyses show that large amounts of excess heat are built up in the NWP during 2043-2057 before rapid releases during 2057-2060 which result in the big jump of record warm GMST. (a) Time series of GMST and the upper 700 m OHC anomalies in the NWP. Dashed line shows the linear trend during 2043-2057. (b) Time series of GMST and the mean dynamic sea level (DSL) in the NWP. (c) Pattern of the 15-year heat accumulation (10^{18} J) in the upper 700 m and the linear trend of wind stress (10^{-3} Pa/year) during 2043-2057. (d) Upper 700 m heat release (negative values) in 2057-2060 and wind stress changes (10^{-2} Pa). (e) and (f) DSL rise and fall (m) associated with this event. More large record-breaking events of GMST with similar mechanisms have been identified in the projections of the CMIP5 models. The results are available upon request.

Table S1. Simulations and projections of 40 CMIP5 models used in the present study. Detailed model and experiment description can be found at http://cmip-pcmdi.llnl.gov/cmip5/.

Model	piControl	Historical	RCP2.6	RCP4.5	RCP6.0	RCP8.5
ACCESS1.0	x	x		x		x
ACCESS1.3	x	x		x		x
bcc-csm1.1	x	x	x	x		x
bcc-csm1.1-m	x	x	x	x	x	x
BNU-ESM		x	x	x		x
CanESM2	x	x	x	x		x
CCSM4	x	x	x	x	x	x
CESM1-BGC	x	x		x		x
CESM1-CAM5	x	x	x	x	x	x
CMCC-CESM	x	x				x
CMCC-CM	x	x		x		x
CMCC-CMS	x	x		x		x
CNRM-CM5	x	x	x	x		x
CSIRO-Mk3.6.0	x	x	x	x	x	
EC-EARTH	x	x	x	x		x
FGOALS-g2	x	x	x	x		x
FIO-ESM	x	x	x	x	x	x
GFDL-CM3	x	x	x	x	x	x
GFDL-ESM2G	x	x	x	x	x	x
GFDL-ESM2M	x	x	x	x	x	x
GISS-E2-H-CC	x	x		x		x
GISS-E2-H	x	x	x	x	x	x
GISS-E2-R-CC	x	x		x		x
GISS-E2-R	x	x	x	x	x	x
HadGEM2-AO		x	x	x	x	x
HadGEM2-CC	x	x		x		x
HadGEM2-ES	x	x	x	x	x	x
inmcm4	x	x		x		x
IPSL-CM5A-LR	x	x	x	x	x	x
IPSL-CM5A-MR	x	x	x	x	x	x
IPSL-CM5B-LR	x	x		x		x
MIROC5		x	x	x	x	x
MIROC-ESM-CHEM	x	x	x	x	x	x
MIROC-ESM	x	x	x	x	x	x
MPI-ESM-LR	x	x	x	x		x
MPI-ESM-MR	x	x	x	x		x
MRI-CGCM3	x	x	x	x	x	x
MRI-ESM1		x				x
NorESM1-ME	x	x	x	x	x	x
NorESM1-M	x	x	x	x	x	x

Table S2. Effective climate sensitivity and internal variability of GMST in the CMIP5 models. Internal variability is evaluated as the standard deviation of the GMST time series in 200-year piControl simulations (the first 200 years available at the CMIP5 archive). The variability of Niño3.4 is also calculated.

Model	Effective Climate Sensitivity (°C)	Internal Variability of GMST (°C)	Internal Variability of Niño3.4 (°C)
ACCESS1.0	3.8	0.12	0.50
ACCESS1.3	3.4	0.09	0.55
bcc-csm1.1	2.8	0.09	–
bcc-csm1.1-m	2.9	0.16	–
BNU-ESM	4.1	–	–
CanESM2	3.7	0.11	0.61
CCSM4	2.9	0.10	0.81
CESM1-BGC	–	0.10	0.87
CESM1-CAM5	–	0.10	0.65
CMCC-CESM	–	0.16	1.20
CMCC-CM	–	0.10	0.58
CMCC-CMS	–	0.11	0.62
CNRM-CM5	3.3	0.11	0.54
CSIRO-Mk3.6.0	4.1	0.12	0.54
EC-EARTH	–	0.10	0.40
FGOALS-g2	3.5	0.07	–
FIO-ESM	–	0.11	0.98
GFDL-CM3	4.0	0.14	0.68
GFDL-ESM2G	2.4	0.12	0.52
GFDL-ESM2M	2.4	0.12	0.89
GISS-E2-H-CC	–	–	0.58
GISS-E2-H	2.3	–	0.62
GISS-E2-R-CC	–	0.08	0.38
GISS-E2-R	2.1	0.07	0.38
HadGEM2-AO	–	–	–
HadGEM2-CC	–	–	0.56
HadGEM2-ES	4.6	0.13	0.59
inmcm4	2.1	0.06	0.39
IPSL-CM5A-LR	4.1	0.11	0.57
IPSL-CM5A-MR	–	0.11	0.61
IPSL-CM5B-LR	2.6	0.11	0.53
MIROC5	2.7	–	–
MIROC-ESM-CHEM	–	0.10	0.42
MIROC-ESM	4.7	0.10	0.42
MPI-ESM-LR	3.6	0.12	0.69
MPI-ESM-MR	3.4	0.09	0.55
MRI-CGCM3	2.6	0.09	0.44
MRI-ESM1	–	–	–
NorESM1-ME	–	0.09	0.69
NorESM1-M	2.8	0.09	0.68